

Multi-scale model for coupled piezoelectric-inelastic behavior

Pablo Moreno-Navarro^{1a}, Adnan Ibrahimbegovic^{*2} and Dragan Damjanovic^{3b}

¹Department of Continuum Mechanics & Theory of Structures, UPV-Universitat Politècnica de València, Valencia, Spain

²UTC-Université de Technologie de Compiègne-Alliance Sorbonne Université, Lab. Roberval, Chaire de Mécanique UTC & IUF Membre Senior, Compiègne, France

³EPFL-Ecole Polytechnique Fédérale de Lausanne, Group for Ferroelectrics and Functional Oxides, Lausanne, Switzerland

(Received October 27, 2021, Revised November 1, 2021, Accepted November 2, 2021)

Abstract. In this work, we present the development of a 3D lattice-type model at microscale based upon the Voronoi-cell representation of material microstructure. This model can capture the coupling between mechanic and electric fields with non-linear constitutive behavior for both. More precisely, for electric part we consider the ferroelectric constitutive behavior with the possibility of domain switching polarization, which can be handled in the same fashion as deformation theory of plasticity. For mechanics part, we introduce the constitutive model of plasticity with the Armstrong-Frederick kinematic hardening. This model is used to simulate a complete coupling of the chosen electric and mechanics behavior with a multiscale approach implemented within the same computational architecture.

Keywords: finite element method; lattice model; multi-scale model; piezoelectricity; Voronoi-cell microstructure representation

1. Introduction

This work seeks to provide a multi-scale strategy for analysis of smart materials and structures, which is very timely effort nowadays. There is a noticeable trend of miniaturization in the state-of-the-art smart materials applications. The smaller these devices are, the more efficient they tend to be due to the control of the microstructure Rowe (2018). Namely, the inclusion of thermoelectric materials in a crystal lattice structure helps improving performance by reducing the thermal conductivity White (2008). Also, this miniaturization has allowed placing an increasing number of sensors and actuators on a structure to monitor and control the current state and structure health.

Numerically, the direct study of macro models is no longer valid to describe the behavior of a structure without a correct homogenization process. The inclusions of devices or materials in the microstructure requires a more detailed study of micro or even nanoscales.

Additionally, the more realistic models for electromagnetics and mechanics induce localizations that are easier to represent in a reliable manner only at a smaller scale.

*Corresponding author, Professor, E-mail: adnan.ibrahimbegovic@utc.fr

^aPh.D., E-mail: pabmona@upv.es

^bProfessor, E-mail: dragan.damjanovic@epfl.ch

There is a large number of references on homogenized solid finite element computation with localized failure and plasticity for mechanics only such as Belytschko *et al.* (1988), Simo *et al.* (1993), Armero and Garikipati (1996), Brancherie and Ibrahimbegovic (2009), Saksala *et al.* (2015), Do *et al.* (2017), Karavelić *et al.* (2019), but none is meant for the problem studied herein.

Different numerical representations of micro-models are available. In terms of numerical efficiency, a structure in terms of Voronoi cell representation with an irregular cohesive discrete lattice model is quite advantageous. This representation is best suited when trying to replicate the multi-scale behavior of a material composed of different micro-behaviors Ostoja Starzewski (2002). The cohesive links are one-dimensional finite elements, such as trusses or beams. This representation can fully replicate the behavior of an equivalent continuum structure Nikolić *et al.* (2018).

In the literature, several papers can be found on the inclusion of embedded discontinuity models in lattice-type structures such as Nikolic and Ibrahimbegovic (2015), Schlangen and Garboczi (1997), Ibrahimbegovic and Delaplace (2003), Ibrahimbegovic and Melnyk (2007), Bui *et al.* (2014). In terms of coupling mechanics with other physics, there are a few references available, for instance, poroplastic media with fluids Hadzalic *et al.* (2019), Nikolic *et al.* (2016), or coupling with thermal field Ngo *et al.* (2013).

Regarding more elaborated constitutive models in terms of ferroelectrics, there are a handful of references that describe this behavior for macro-scale in a similar fashion as plasticity, such as Miehe *et al.* (2011), McMeeking and Landis (2002), Huber *et al.* (1999), McMeeking and Hwang (1997). Other references focus on the behavior of the crystals at a micro-scale level, for example Hwang *et al.* (1995), Chen and Lynch (1998). A complete description on the typical ferroelectric hysteresis loops can be found in Damjanovic (2006), including the description of Debye models, such as Palma *et al.* (2018). References on multi-scale modeling of ferroelectrics and ferromagnetics can be found as well in the literature like Labusch *et al.* (2016), Daniel *et al.* (2004, 2008, 2014), among others.

The main objective and novelty of this work is to obtain a numerical model for lattice of beams to replicate the micro behavior of a ferroelectric grain. The proposed model also implements a non-linear viscoplasticity. The remanent polarization is also described, following Hwang *et al.* (1995), as a constant value added on top of the linear electric displacement. A polarization multiplier determines the evolution of the remanent polarization and strain. Each beam pictures a grain of the material. Therefore, the lattice model produces the macro response of a heterogeneous ferroelectric model. This response can be obtained by averaging the internal values of the system, or through a process of homogenization where the stiffness terms are created by a consistent interpolation Rukavina *et al.* (2019).

All the numerical implementations and computations are carried out with the computer code FEAP-Finite Element Analysis Program Zienkiewicz and Taylor (2005). This code has been developed at the University of Berkeley, California, by Prof. R.L. Taylor.

The outline of the paper is as follows. In Section 2, we briefly present basic lattice model for mechanics. Its extension for ferroelectrics is given in Section 3. The numerical implementation is described in Section 4. Several numerical simulations are given in Section 5. Concluding remarks are stated in Section 6.

2. Basics of a lattice-type model

To create a model of this type, the domain to study is divided into polyhedral regions. The

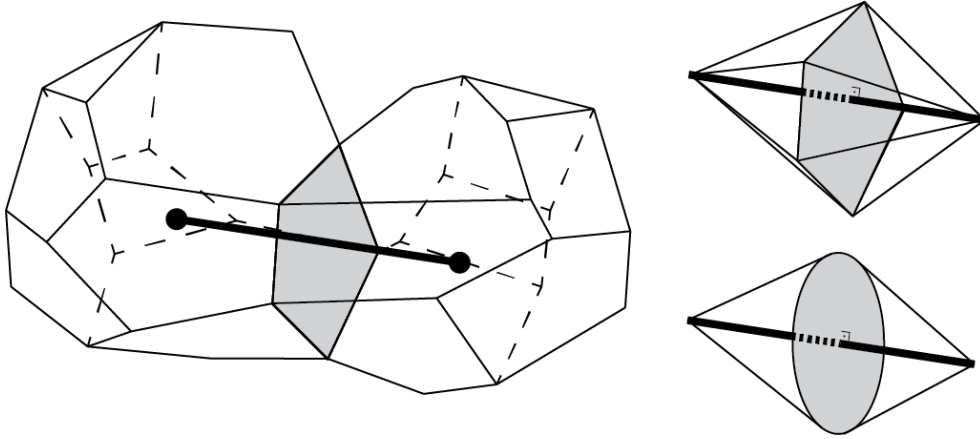


Fig. 1 Left, two adjacent Voronoi cells held together by the corresponding lattice model. Right, the assumed shape of the beam and the approximation of the circular cross-section

circumcenter of each polyhedron, defined as the point that is located at the same distance of each vertex of the polyhedron and the center of the circumscribed sphere, constitutes one of the ends of the lattice beam. Two adjacent Voronoi cells are held together with a lattice beam which is chosen as a beam Nikolić *et al.* (2018), Bui *et al.* (2014).

In Fig. 1 left, two adjacent cells, and the corresponding lattice beam are pictured. As a property of the circumcenter, the beam is perpendicular to the joint face of these two cells. Also, the face intersects in the middle of the beam, dividing it into two halves.

The transversal area associated with this beam is the area of the joint face, a polygon, as depicted in Fig. 1 right. The transversal area is assumed to be an equivalent circle with the same area to simplify the calculation of the beam properties. The lattice beams define the dual mesh of the Voronoi cell. Delaunay algorithms for the creation of tetrahedron are used to create the mesh of beams that will be used to solve the problem.

2.1 Notation for beam model

The selected model for the beam is in agreement with Timoshenko hypotheses, where the transversal sections can be rotated with respect to the normal of the neutral line. The degrees of freedom for the mechanic field are three displacements and three rotations:

$$\mathbf{u} = (u_1, u_2, u_3, \varphi_1, \varphi_2, \varphi_3)^T$$

The generalized strain measures are ordered in a vector:

$$\boldsymbol{\varepsilon} = (\varepsilon_1, \gamma_{12}, \gamma_{13}, \kappa_1, \kappa_2, \kappa_3)^T$$

The corresponding internal force vector:

$$\mathbf{F} = (N_1, N_2, N_3, M_1, M_2, M_3)^T$$

Regarding the electric field, the only degree of freedom is the electric potential V . For the beam model, only the axial component x_1 is relevant; thus, by definition, the electric field E_1 and the electric displacement D_1 are scalars along any lattice. Assuming the homogeneity of any variable within every section, we can define the electric charge as $Q_1 = D_1 A$, with A as the cross-section area of the beam.

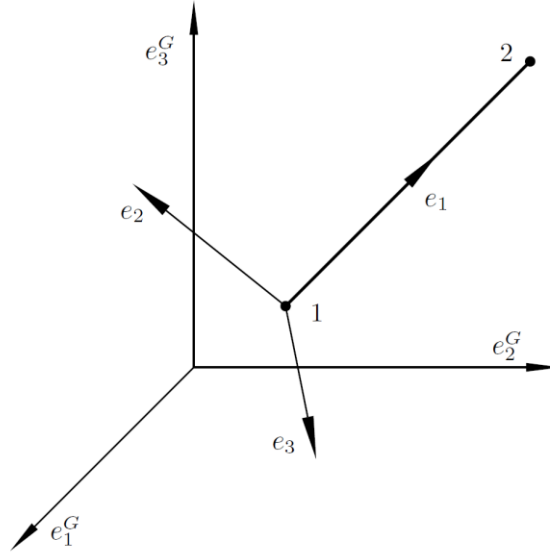


Fig. 2 Local frame representation for a beam. The local direction 1 is oriented from local node 1 to 2. Local directions 2 and 3 are randomly chosen, but remain perpendicular to the beam axis

A point on the beam can also be represented in global coordinates as:

$$\tilde{\mathbf{x}} = (\tilde{x}_1, \tilde{x}_2, \tilde{x}_3)^T$$

where the tilde overscript \sim is used in this section to describe that the corresponding variable is expressed in the global orthonormal basis. This basis is composed of base unit vectors \mathbf{e}_i^G for every direction i . The point can also be expressed in beam local coordinates as:

$$\mathbf{x} = (x_1, x_2, x_3)^T$$

Notice that the overscript omitted from the notation means that the vector is expressed in local coordinates. This local basis is comprised of base unit vectors \mathbf{e}_i for every direction i . The axial direction of the beam is always the first one. Since the beam section is considered circular, transverse directions are taken randomly and normal to the axial direction, in agreement with the right-hand rule, as illustrated in Fig. 2.

The rows of the transformation matrix \mathbf{T} are the base unit vectors \mathbf{e}_i expressed in global coordinates:

$$\mathbf{T} = \begin{pmatrix} \leftarrow & \tilde{\mathbf{e}}_1^T & \rightarrow \\ \leftarrow & \tilde{\mathbf{e}}_2^T & \rightarrow \\ \leftarrow & \tilde{\mathbf{e}}_3^T & \rightarrow \end{pmatrix}$$

This transformation matrix is used to change the basis in which every variable is denoted. In general, a tensor \mathbf{A} of any order is expressed in global coordinates as:

$$\tilde{A}_{ijkl\dots} = T_{Ii}T_{Jj}T_{Kk}T_{Ll}\dots A_{IJKL\dots}$$

2.2 Kinematic equations

Kinematic equations relate displacement and voltage degrees of freedom with generalized strains

defining the state or primal variables. For a solid continuum model with the hypothesis on small displacements, the corresponding equations that define the infinitesimal strain tensor and the electric field vector are:

$$\varepsilon = \frac{1}{2}[\nabla \otimes \mathbf{u} + (\nabla \otimes \mathbf{u})^T] = \nabla^{\text{sy}} \mathbf{u}$$

$$\mathbf{E} = -\nabla V$$

To obtain the reduced model for a Timoshenko beam, we need to take into account that every variable only changes in axial direction. Thus, the only relevant strain components are the axial strain ε and transversal shears γ_{12} and γ_{13} , as well as the axial electric field E_1 , each one constant within the beam cross-section. Besides, as a consequence of the additional degrees of freedom for the mechanic field, curvatures κ_1, κ_2 , and κ_3 have to be calculated. These assumptions will further specialize when considering the Timoshenko kinematic model Bui *et al.* (2014), the continuum version of (8) reduces to:

$$\begin{pmatrix} \varepsilon_1 \\ \gamma_{12} \\ \gamma_{13} \\ \kappa_1 \\ \kappa_2 \\ \kappa_3 \\ E_1 \end{pmatrix} = \begin{bmatrix} \frac{\partial}{\partial x_1} & 0 & 0 & 0 & 0 & 0 & 0 \\ 0 & \frac{\partial}{\partial x_1} & 0 & 0 & 0 & -1 & 0 \\ 0 & 0 & \frac{\partial}{\partial x_1} & 0 & 1 & 0 & 0 \\ 0 & 0 & 0 & \frac{\partial}{\partial x_1} & 0 & 0 & 0 \\ 0 & 0 & 0 & 0 & \frac{\partial}{\partial x_1} & 0 & 0 \\ 0 & 0 & 0 & 0 & 0 & \frac{\partial}{\partial x_1} & 0 \\ 0 & 0 & 0 & 0 & 0 & 0 & \frac{\partial}{\partial x_1} \end{bmatrix} \begin{pmatrix} u_1 \\ u_2 \\ u_3 \\ \varphi_1 \\ \varphi_2 \\ \varphi_3 \\ V \end{pmatrix}$$

2.3 Conservation equations

Conservation principles are used for defining the equilibrium in a material, which are defined in terms of partial differential equations. The solid version of these equations is expressing equilibrium of mechanical forcer and electric field in the absence of external charges. For this beam model, the main hypotheses assumed are that body forces are neglected and a quasi-static approach is taken.

$$\sigma \nabla = 0$$

$$\nabla \cdot \mathbf{D} = 0$$

The adaptation for the beam model includes the hypotheses in the previous section regarding one-dimensionality and homogeneity of variables in a transversal section. Thus, the simplified version of equilibrium equations for beams reduces to:

$$\frac{\partial N_i}{\partial x_1} = 0;$$

$$\frac{\partial M_i}{\partial x_1} = 0;$$

$$\frac{\partial Q_1}{\partial x_1} = 0$$

2.4 Constitutive equations for piezoelectricity

Constitutive equations will relate the primal variables with stress or flow variables as thermodynamic duals through the given defined material properties. In the case of piezoelectric materials, in addition to the conventional relationship between the same kind of variables, electrical variables affect the behavior of the mechanical ones and vice-versa. The constitutive equations can be derived from the free-energy potential as defined in Moreno-Navarro *et al.* (2018), from which we can retrieve:

$$\begin{aligned}\sigma &= C\varepsilon - e^e E \\ D &= \epsilon E + e^e \varepsilon\end{aligned}$$

The coefficients used in (12) are the fourth-order stiffness tensor \mathbf{C} , the third-order piezoelectric tensor e^e , and the second-order permittivity tensor ϵ , all of them obtained for assumed material properties of piezoelectricity.

To reduce such constitutive model to beams, we need to account for the simplification made in the last sections. First, only a few components of primal variables are relevant, so are the corresponding material tensor entries. Second, the addition of rotational degrees of freedom for the mechanic field introduces new structural variables into the stiffness tensor. Finally, only axial strain affects the axial electric variables and vice-versa. With these assumptions in hand, we can write the beam-model version of (12):

$$\begin{pmatrix} N_1 \\ N_2 \\ N_3 \\ M_1 \\ M_2 \\ M_3 \\ Q_1 \end{pmatrix} = \begin{bmatrix} \check{E}A & 0 & 0 & 0 & 0 & 0 & -e_{11}A \\ 0 & k_c GA & 0 & 0 & 0 & 0 & 0 \\ 0 & 0 & k_c GA & 0 & 0 & 0 & 0 \\ 0 & 0 & 0 & GJ & 0 & 0 & 0 \\ 0 & 0 & 0 & 0 & \check{E}I & 0 & 0 \\ 0 & 0 & 0 & 0 & 0 & \check{E}I & 0 \\ e_{11}A & 0 & 0 & 0 & 0 & 0 & \epsilon_1 A \end{bmatrix} \begin{pmatrix} \varepsilon_1 \\ \gamma_{12} \\ \gamma_{13} \\ \kappa_1 \\ \kappa_2 \\ \kappa_3 \\ E_1 \end{pmatrix}$$

where $\check{E} = E(1 - \nu)/[(1 + \nu)(1 - 2\nu)]$ is the first term of the stiffness tensor (with E as the Young's modulus and ν as the Poisson's coefficient), k_c is the shear correction factor, G is the shear modulus, J is the polar moment of inertia, I is the moment of inertia, ϵ_1 is the permittivity in axial direction, and e_{11} is the piezoelectric coefficient. Notice that inertia moments are the same for x_2 and x_3 directions, and $k_c \approx 0.9$ since the transversal area is considered a circle.

3. Ferroelectric model

The beams used in this section have a more elaborated constitutive model than the one presented in (13). This model introduces non-linear relations in mechanics (viscoplasticity) and electricity (ferroelectricity). A complete description of these constitutive models is presented herein.

Polarization \mathbf{P} is a macroscopic magnitude that accumulates the microscopic electric dipole moments in a material. These dipoles are either generated in the presence of an electric field or as a consequence of a particular microstructure. While the former is proportional to the electric field applied, the latter is a permanent value, usually called remanent polarization P^r , with the only possibility of a change of orientation or domain switching Balanis (1999).

In general, there are three types of macroscopic behavior regarding polarization: dielectric, paraelectric and ferroelectric. For the first one, the polarization is linear to the electric field applied;

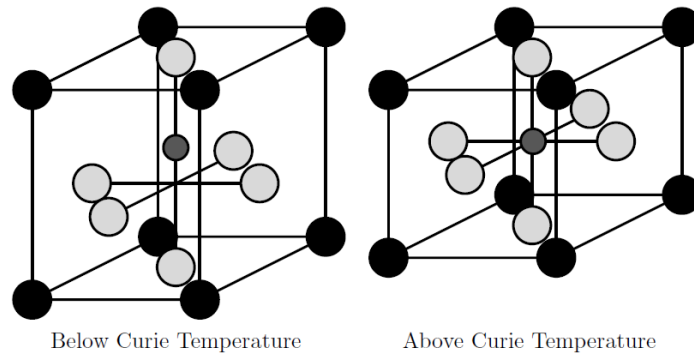


Fig. 3 Sketch of a tetragonal unit cell for PbTiO_3 below (tetragonal) and above (cubic) Curie temperature. Pb in black, O in white and Ti in gray

the second one depends on the electric field as well, but the dependency is non-linear; finally, ferroelectrics have a dependency on the electric field and, superposed, the remanent polarization causing hysteresis phenomena to arise. Ferroelectricity implies always a coupling with the mechanical field, since only piezoelectric materials can be ferroelectrics. In fact, they also have to be pyroelectric, but we are not considering in this chapter that kind of coupling Said *et al.* (2017).

The appearance of this remanent polarization can be explained clearly from a microstructure point-of-view. In this chapter, only polarizable tetragonal cell materials are being discussed De Jong *et al.* (2015). A representative unit cell of this type is sketched in Fig. 3 for PbTiO_3 with the different microstructure arrangements depending on the temperature. Below the Curie temperature T_c , the microstructure is tetragonal, and it behaves as ferroelectric; above this temperature, the microstructure is cubic, the remanent polarization is gone, and its behavior is paraelectric.

The atoms in the center (Ti, in gray) and the corners (Pb, in black) are charged positively while the ones in the middle of the faces are charged negatively (O, in white). Above the Curie temperature, the cell is perfectly symmetric and cubic, with Ti in the center. Below the Curie temperature, the cell reaches minimum potential energy if Ti is ousted from the center in a direction towards one of the oxygen atoms.

This eccentricity creates a microscopic electric dipole due to the misalignment compared with the cubic structure. Notice as well that the cell has been enlarged in the same direction of the misalignment since Ti repels the top O. If the position of Ti switches to any of the other five equilibrium positions, the remanent polarization and the cell enlargement will change as well.

A strong electric field has to be applied in the desired direction to switch the central atom into any of the other minimum positions. This position is also modified if a compressive stress is applied in the direction of the current remanent polarization or traction in any of the corresponding transversal directions. The angle between the old and the new vector \mathbf{P}^r determines the two types of switching: 180° and 90° . An oriented electric field can cause both 180° and 90° switches, whereas stress can only generate a 90° switch.

The selected criteria to determine whether a switch occurs are extracted from Keip and Schröder (2011) with the combination of both electric field and stress taken into account. Each switch criterion is cast as an energy criterion at a microscopic level, and several possibilities have to be evaluated at the same time for both kinds of switch. Namely, a switch can take place if the following conditions meet:

$$\frac{\mathbf{E} \cdot \Delta \mathbf{P}^r}{2\mathbf{E} \cdot \mathbf{P}^s} \geq 1, \text{ for } 180^\circ \text{ switch}$$

$$\frac{\mathbf{E} \cdot \Delta \mathbf{P}^r}{\mathbf{E} \cdot \boldsymbol{\varepsilon}^s} + \frac{\boldsymbol{\sigma} \cdot \Delta \boldsymbol{\varepsilon}^r}{\boldsymbol{\sigma} \cdot \boldsymbol{\varepsilon}^s} \geq 1, \text{ for } 90^\circ \text{ switch}$$

where the increments $\Delta \mathbf{P}^r$ and $\Delta \boldsymbol{\varepsilon}^r$ are respectively the tensors of change for remanent polarization and strain, while \mathbf{P}^s and $\boldsymbol{\varepsilon}^s$ are respectively the spontaneous values of remanent polarization and strain induced by internal microstructure. We note that the above conditions need to be evaluated for each of the five alternative directions of polarization.

Any such switch introduces a change in the microstructure and alters the isotropy of the material, making it transversally isotropic with a preferential direction in the remanent polarization orientation. In Labusch *et al.* (2016), the authors provide a comprehensive description of the enthalpy for magneto-electro-mechanical polarizable materials at a microscale model. We obtain the corresponding constitutive equations through the derivation of the enthalpy with respect to the dual variables. Since this definition of enthalpy is quadratic, the constitutive coefficients are constant. A switch in polarization makes these coefficients to change their value.

As in the previous solid model for our beam lattice model, the coefficients in (13) are also subjected to change with every polarization switch, which implies a change in \check{E} , G , e_{11} , and ϵ_1 . The factor that modifies these properties from its non-polarized to its polarized value is the polarization multiplier m defined through the following linear distributions:

$$\begin{aligned}\check{E} &= \check{E}^{np} + |m|(\check{E}^p - \check{E}^{np}) \\ G &= G^{np} + |m|(G^p - G^{np}) \\ e_{11} &= e_{11}^{np} + m(e_{11}^p - e_{11}^{np}) \\ \epsilon_1 &= \epsilon_1^{np} + |m|(\epsilon_1^p - \epsilon_1^{np})\end{aligned}$$

where the superscripts np and p stand for non-polarized and polarized values of each coefficient and $|m|$ stands for the absolute value of m . The values for remanent polarization and remanent strain are also a function of this multiplier as defined as follows:

$$\begin{aligned}P_1^r &= mP_1^s \\ \varepsilon_1^r &= \varepsilon_1^{np} + |m|(\varepsilon_1^p - \varepsilon_1^{np})\end{aligned}$$

The activation of these remanent variables modify the constitutive equation (13) in the following way:

$$\begin{pmatrix} N_1 \\ N_2 \\ N_3 \\ M_1 \\ M_2 \\ M_3 \\ Q_1 \end{pmatrix} = \begin{bmatrix} \check{E}A & 0 & 0 & 0 & 0 & 0 & -e_{11}A \\ 0 & k_cGA & 0 & 0 & 0 & 0 & 0 \\ 0 & 0 & k_cGA & 0 & 0 & 0 & 0 \\ 0 & 0 & 0 & GJ & 0 & 0 & 0 \\ 0 & 0 & 0 & 0 & \check{E}I & 0 & 0 \\ 0 & 0 & 0 & 0 & 0 & \check{E}I & 0 \\ e_{11}A & 0 & 0 & 0 & 0 & 0 & \epsilon_1A \end{bmatrix} \begin{pmatrix} (\varepsilon_1 - \varepsilon_1^r) \\ \gamma_{12} \\ \gamma_{13} \\ \kappa_1 \\ \kappa_2 \\ \kappa_3 \\ E_1 \end{pmatrix} + \begin{pmatrix} 0 \\ 0 \\ 0 \\ 0 \\ 0 \\ 0 \\ P_1^rA \end{pmatrix}$$

Two models to represent the switching of polarization and to define the polarization multiplier are presented here. For the first one, the only switch considered is the 180° since beams lattice can only take into account axial variations in voltage. Therefore, 90° switches are not possible to simulate, the strain is not a factor for m , and a compressive force cannot depolarize the beam in axial direction.

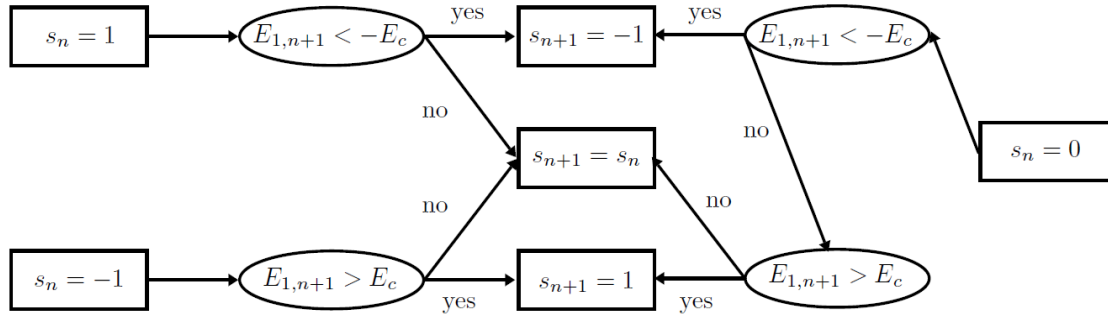


Fig. 4 Flowchart to select the switch-state for the next time step s_{n+1} based on its previous value s_n and the current value of electric field E_{n+1}

A more refined version of this model requires a small variation to take into account the effect of compression and traction in the bar. The idea is to include a third state of the switch of no remanent polarization as the replacement for 90° switching. This way, every beam can take three states: positive, negative, and no axial remanent polarization or zero polarization. This can be enforced as a constraint in the same manner as modeling the inextensible beam deformation Medić *et al.* (2013).

A numerical difficulty arises when the switch in polarization is implemented as a Heaviside step once one of the conditions in (14) is met. This abrupt change can lead to oscillating residual norms in the finite element method computations due to the uncertainty in a scenario with one or more of the beams getting simultaneously polarized. Such computational difficulty is handled with a smooth correction to this Heaviside step proposed for these two models through the hyperbolic tangent function. The idea is to make a bijective function between electric field and electric displacement, removing any possible uncertainty and introducing a rapid yet smooth change of slope. Once the polarization switches, the constitutive model changes to represent hysteresis behavior.

3.1 Switching model 1

The flowchart for the switching model 1 is depicted in Fig. 4. In this model, every beam starts with the zero switch-state $s_n = 0$, where subscript n denotes that the variable is taken at time t_n . It will remain in this state until the beam reaches the coercive electric field E_c or $-E_c$. This forces the switch-state to change in the next time step to either $s_{n+1} = 1$ or $s_{n+1} = -1$, denoting positive or negative polarization respectively. After the beam is polarized, the beam can only switch to the opposite polarized state (180°) once it reaches the opposite value of the coercive electric field, i.e., either $-E_c$ for $s_n = 1$ or E_c for $s_n = -1$.

Even though the three states of polarization are implemented in this model, we make the restriction that once a beam is polarized either positive or negative, it cannot return to the zero-state. This first model is quite simple; yet, it allows us to obtain a good approximation in macroscopic electric displacement \mathbf{D} .

Although the switch-state changes suddenly as a step function, the polarization multiplier is in fact chosen as a smooth function, continuous, and differentiable, cast in terms of the hyperbolic tangent. This regularized multiplier depends on the current axial electric field in the beam $E_{1,n+1}$ and the switch from the previous time step s_n , which is defined as follows:

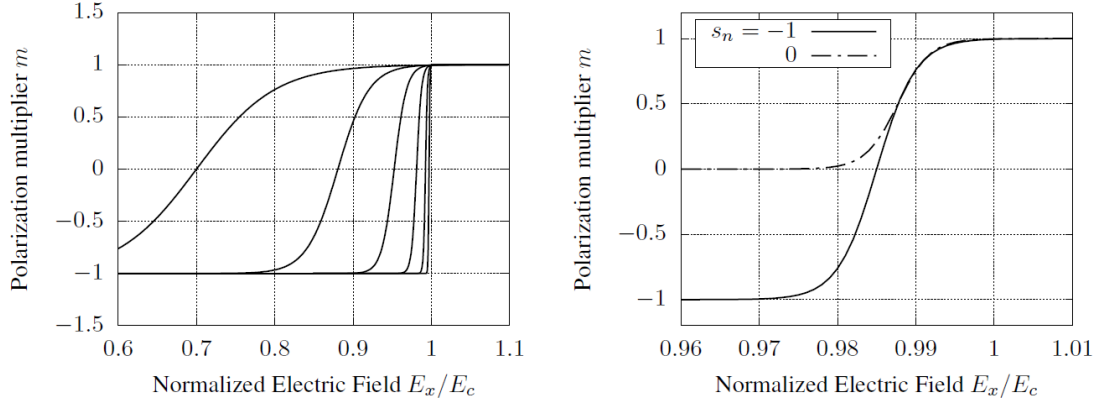


Fig. 5 Left, smoothed polarization multiplier m curves for negative switch-state $s_n = -1$ with different values of parameter $a = \{10, 25, 60, 160, 400, 1000\}$. Right, detail of curves with chosen value $a = 200$ for $|s_n| = 1$ and $a = 244$ for $s_n = 0$

$$m_{n+1}(E_{1,n+1}, s_n) = \frac{1 - s_n}{2} \tanh \left[\frac{a(s_n)}{E_c} (E_{1,n+1} - E_c) + 3 \right] + \frac{1 + s_n}{2} \tanh \left[\frac{a(s_n)}{E_c} (E_{1,n+1} + E_c) - 3 \right]$$

In terms of the hyperbolic tangent is a function with odd symmetry such as a smoothed version of a Heaviside step, with horizontal asymptotic values of -1 and 1 for the former instead of 0 and 1 for the latter. In our case, the chosen form of the argument is $a/|x_0|(x \mp |x_0|) \pm 3$. The last number has been selected in agreement with $\tanh(3) = -\tanh(-3) \approx 0.995$ to translate the function so that when $|x| > |x_0|$ we can consider that the function has already arrived at the other asymptotic value.

In (18), the normalized parameter $a(s_n)$ controls how smooth or how sharp the curve is as illustrated in Fig. 5 left, where the value of $s_n = -1$ has been adopted. The higher the value of a is, the more similar to a Heaviside step function the regularized polarization multiplier is. The decision for taking such value of a is representative of a crystal with m that starts to change from one asymptotic value to the next one. For this model, we adopted a value of $a = 200$ for $s_n = \pm 1$ that corresponds to $m \approx \pm 0.995$ when $E_{1,n+1} = \mp 0.97E_c$. If $s_n = 0$ then we choose $a = 244$ to adjust the final part of the curve to the one with polarization as illustrated in Fig. 5 right.

The polarization multiplier curves for the three switch-states are drawn in Fig. 6 left, where the typical hysteresis loop for ferroelectric materials can be observed Hwang *et al.* (1995). The choice of parameters for this model makes the behavior of variables affected by polarization very similar to the Heaviside step. Hence, the derivative with respect to the electric field is comparable to the Dirac delta function, as can be seen in the detail of Fig. 6 right.

3.2 Switching model 2

Switching model 2 is capable of representing the depolarization of the beams since the switching criteria include the dependency on mechanical stress. The flowchart for this model is depicted in Fig. 7.

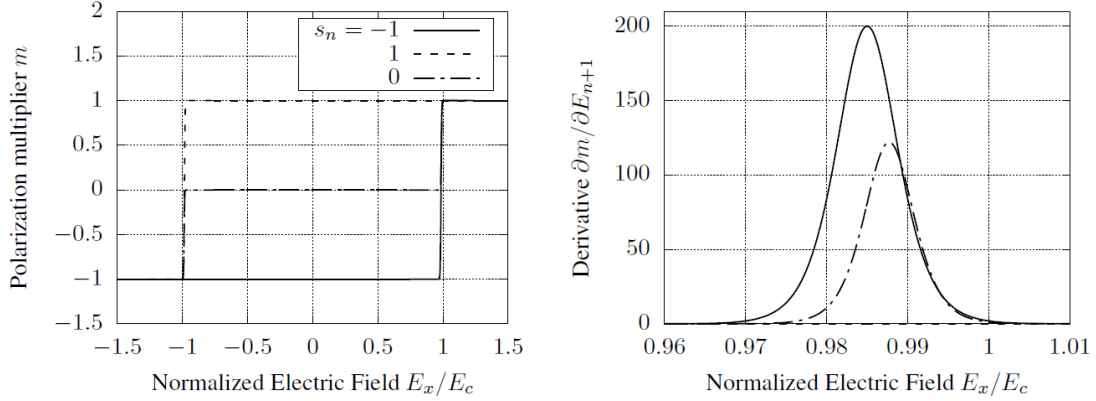


Fig. 6 Left, smoothed polarization multiplier m curves for all three previous state of polarization s_n with the chosen $a = 200$. Right, detail of the corresponding derivatives of m with respect to the electric field

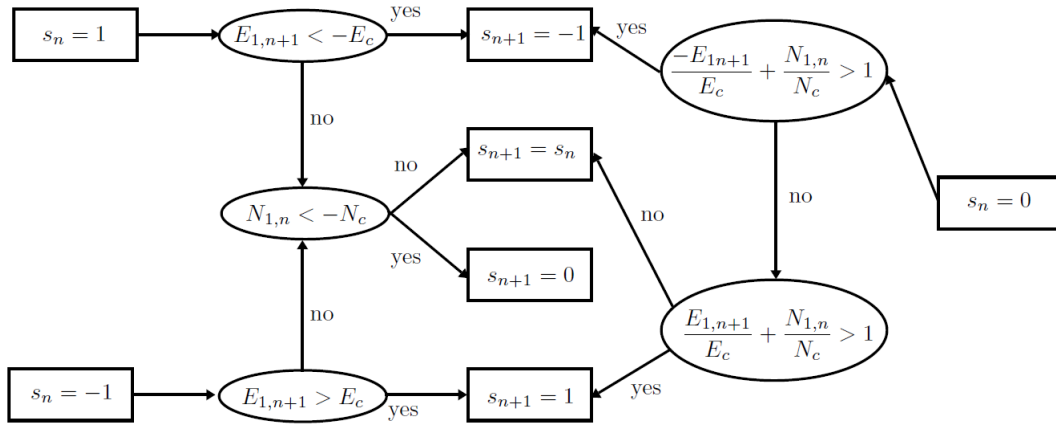


Fig. 7 Flowchart to select the switch for the next time step based on the previous state of switch s_n , the current value of electric field E_{n+1} , and the previous value of axial force $N_{1,n}$

Every beam starts with the zero switch-state $s_n = 0$. A 90° switching condition is tested to check if the beam is getting polarized in the main axial directions:

$$s_{n+1} = -1; \text{ if } \frac{-E_{1,n+1}}{E_c} + \frac{N_{1,n}}{N_c} > 1$$

$$s_{n+1} = 1; \text{ if } \frac{E_{1,n+1}}{E_c} + \frac{N_{1,n}}{N_c} > 1$$

This condition is derived from (14) combined with the beam model hypotheses. Once the beam gets polarized into one of the axial directions, both 180° and 90° switchings can happen. The former can be reached only with a significant change in electric variables. As for the latter, only mechanical variables are relevant since electric variables are non-zero in any transversal direction. The switching criterion is the simplified version of (14). Namely, for $s_n = 1$

$$s_{n+1} = -1; \quad \text{if } E_{1,n+1} < -E_c$$

$$s_{n+1} = 0; \quad \text{if } N_{1,n} < -N_c$$

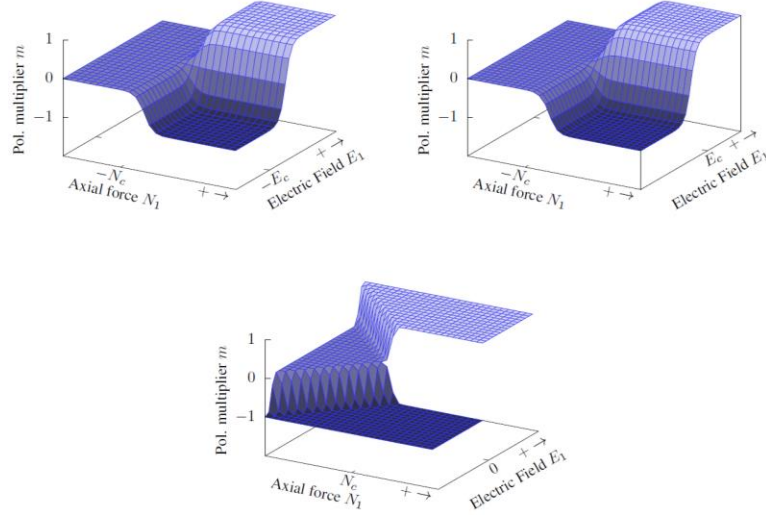


Fig. 8 Smoothed polarization multiplier m curves for switching model 2 with different values of the previous switching state $s_n = 1$ for top left, $s_n = -1$ for top right, and $s_n = 0$ for bottom figure

Whereas for $s_n = -1$:

$$\begin{aligned} s_n &= 1; & \text{if } E_{1,n+1} > E_c \\ s_n &= 0; & \text{if } N_{1,n} < -N_c \end{aligned}$$

One can notice that these criteria, once the beam is polarized in any of the axial directions, are decoupled. i.e., 90° switching depends only on the mechanic stress, while 180° switching depends only on the electric field. We observe as well that the axial force is considered at the previous time step in order to simplify the recursive calculation of local variables. An iterative method to obtain the current axial force could be developed, but the assumption is that the time step is small enough to consider major differences between previous and current values.

The regularized polarization multiplier for this model is created similarly to the one in the previous model by using the hyperbolic tangent function. The main difference is that, for every polarization state, there is a different expression:

$$\begin{aligned} m_{n+1}(E_{1,n+1}, N_{1,n}) &= \frac{1}{2} \left\{ 1 + \tanh \left[\frac{a(0)}{N_c} (N_{1,n} + N_c) - 3 \right] \right\} \\ &\quad \tanh \left[\frac{a(1)}{E_c} (E_{1,n+1} + E_c) - 3 \right]; \text{ if } s_n = 1 \\ m_{n+1}(E_{1,n+1}, N_{1,n}) &= \frac{1}{2} \left\{ 1 + \tanh \left[\frac{a(0)}{N_c} (N_{1,n} + N_c) - 3 \right] \right\} \\ &\quad \tanh \left[\frac{a(1)}{E_c} (E_{1,n+1} - E_c) + 3 \right]; \text{ if } s_n = -1; \\ m_{n+1}(E_{1,n+1}, N_{1,n}) &= \frac{\text{sign}(E_{1,n+1})}{2} \left\{ 1 + \right. \\ &\quad \left. \tanh \left[a(0) \left(\frac{|E_{1,n+1}|}{E_c} + \frac{N_{1,n}}{N_c} - 1 \right) + 3 \right] \right\}; \text{ if } s_n = 0 \end{aligned}$$

In Fig. 8, all three polarization multiplier situations are illustrated, with $E_{1,n+1}$ and $N_{1,n}$ as the independent variables. The change of value for m takes place near the coercive values E_c or N_c for the axial polarization state with the same smoothed pattern as in the previous model. As for the depolarized beam, the combined criterion creates a diagonal line of values that nullify the argument of the hyperbolic tangent. Notice that near $E_{1,n+1} = 0$ there is a jump for the polarization multiplier, which should not affect the stability of the element since once $m_{n+1} \approx \pm 1$, the polarization state switches to the other corresponding criteria.

3.3 Viscoplasticity model

The proposed mechanic model will change once the material has reached the yield stress. Here, we adapt to the one-dimensional beam model framework the viscoplasticity with Armstrong-Frederick non-linear kinematic hardening (proposed in Ibrahimbegovic 2009). This model is implemented independently both for the axial strain and the two shear strains. The description of this constitutive model starts with the hypothesis of additive decomposition of the strains into elastic, plastic, and remanent parts induced by polarization only taken for the case of axial strain:

$$\bar{\varepsilon}_1 = \varepsilon_1^e + \varepsilon_1^{vp} + \varepsilon_1^r; \bar{\gamma}_{12} = \gamma_{12}^e + \gamma_{12}^{vp}; \bar{\gamma}_{13} = \gamma_{13}^e + \gamma_{13}^{vp}$$

where the bar indicates the total regular part of the total strains, superscript e denotes the elastic part, vp the viscoplastic part, and r the remanent part. We note in passing that the curvatures κ_i are kept elastic considering they are not affected by the viscoplasticity in ferroelectric model. Also, the electric charge is split into elastic and remanent (saturated polarization) parts according to $Q_1 = Q_1^e + P_1^r$. Consequently, the free energy potential ψ is decomposed into three decoupled terms:

$$\begin{aligned} \bar{\psi}_1(\varepsilon_1^e, \bar{\zeta}_1, E_1) &= \frac{1}{2} \varepsilon_1^e \check{E} \varepsilon_1^e + \frac{1}{2} \bar{\zeta}_1 H_{is,1} \bar{\zeta}_1 - e_{11} \varepsilon_1^e E_1 - \frac{1}{2} E_1 \varepsilon_1 E_1 \\ \bar{\psi}_2(\gamma_{12}^e, \bar{\zeta}_2) &= \frac{1}{2} \gamma_{12}^e k_c G \gamma_{12}^e + \frac{1}{2} \bar{\zeta}_2 H_{is,2} \bar{\zeta}_2 \\ \bar{\psi}_3(\gamma_{13}^e, \bar{\zeta}_3) &= \frac{1}{2} \gamma_{13}^e k_c G \gamma_{13}^e + \frac{1}{2} \bar{\zeta}_3 H_{is,3} \bar{\zeta}_3 \end{aligned}$$

The total dissipation is defined through the standard procedure (e.g., Ibrahimbegovic 2009), applying the second principle of thermodynamics, and the Legendre transformation in order to the internal energy to exchange the role of Q_1 and E_1 :

$$\begin{aligned} \bar{\mathcal{D}}_1 &= -\dot{\bar{\psi}}_1 - \frac{1}{A} \frac{\partial(Q_1^e E_1)}{\partial t} + \frac{N_1}{A} \dot{\varepsilon}_1 + \frac{Q_1}{A} \dot{E}_1 = \frac{N_1}{A} (\dot{\varepsilon}_1^{vp} + \dot{\varepsilon}_1^r) + \bar{q}_1 \dot{\bar{\zeta}}_1 + E_1 \frac{\dot{P}_1^r}{A} \\ \bar{\mathcal{D}}_2 &= -\dot{\bar{\psi}}_2 + \frac{N_2}{A} \dot{\gamma}_{12} = \frac{N_2}{A} \dot{\gamma}_{12}^{vp} + \bar{q}_2 \dot{\bar{\zeta}}_2 \\ \bar{\mathcal{D}}_3 &= -\dot{\bar{\psi}}_3 + \frac{N_3}{A} \dot{\gamma}_{13} = \frac{N_3}{A} \dot{\gamma}_{13}^{vp} + \bar{q}_3 \dot{\bar{\zeta}}_3 \end{aligned}$$

In order to get the final result defined by the previous expressions, the following constitutive relations have been enforced:

$$\begin{aligned} N_1 &= A \frac{\partial \bar{\psi}_1}{\partial \varepsilon_1^e}; N_2 = A \frac{\partial \bar{\psi}_2}{\partial \gamma_{12}^e}; N_3 = A \frac{\partial \bar{\psi}_3}{\partial \gamma_{13}^e}; Q_1^e = -A \frac{\partial \bar{\psi}_1}{\partial E_1} \\ \bar{q}_1 &= -\frac{\partial \bar{\psi}_1}{\partial \bar{\zeta}_1}; \bar{q}_2 = -\frac{\partial \bar{\psi}_2}{\partial \bar{\zeta}_2}; \bar{q}_3 = -\frac{\partial \bar{\psi}_3}{\partial \bar{\zeta}_3} \end{aligned}$$

where each \bar{q}_i is the stress-resultant hardening variable in direction i . The viscoplastic part of the dissipation is extracted from (25) by removing the remanent part of the strain and the polarization terms because they are governed by different evolution equations as described in the previous section. The yield functions governing the change of viscoplastic dissipation are chosen following Ibrahimbegovic (2009) and Ibrahimbegovic (1997) as:

$$\bar{\phi}_i = |N_i - \chi_i A| - (N_{i,y} - \bar{q}_i A)$$

where $N_{i,y}$ is the yield stress-resultant in direction i , and χ_i is the backstress in direction i . The corresponding evolution equation and stress-resultant equivalent to those defined for the Armstrong-Frederick model in terms of implicit differential equations:

$$\begin{aligned}\dot{\chi}_1 &= H_{l,1} \dot{\varepsilon}_1^{\text{vp}} - H_{n,1} \dot{\zeta}_1 \chi_1 \\ \dot{\chi}_2 &= H_{l,2} \dot{\gamma}_{12}^{\text{vp}} - H_{n,2} \dot{\zeta}_2 \chi_2 \\ \dot{\chi}_3 &= H_{l,3} \dot{\gamma}_{13}^{\text{vp}} - H_{n,3} \dot{\zeta}_3 \chi_3\end{aligned}$$

The principle of maximum viscoplastic dissipation can be applied to obtain the final evolution equations of the viscoplastic variables by introducing the corresponding regularized Lagrangian (e.g., Ibrahimbegovic 2009). The main difference with respect to plasticity is that the values of $\bar{\phi}_i > 0$ are admissible but with penalizing positive values of the yield function proportional to the inverse of the viscosity coefficient η_i as follows:

$$\begin{aligned}\bar{\mathcal{L}}_1 &= -\bar{\mathcal{D}}_1^{\text{vp}} + \frac{\langle \bar{\phi}_1 \rangle}{\eta_1} \\ \bar{\mathcal{L}}_2 &= -\bar{\mathcal{D}}_2^{\text{vp}} + \frac{\langle \bar{\phi}_2 \rangle}{\eta_2} \\ \bar{\mathcal{L}}_3 &= -\bar{\mathcal{D}}_3^{\text{vp}} + \frac{\langle \bar{\phi}_3 \rangle}{\eta_3}\end{aligned}$$

where $\langle \cdot \rangle$ is the Macaulay bracket, an operator defined as $\langle \phi \rangle = \phi$ if $\phi > 0$ and $\langle \phi \rangle = 0$ otherwise. The evolution of the viscoplastic variables can then be calculated:

$$\begin{aligned}\frac{\partial \bar{\mathcal{L}}_1}{\partial N_1} &= -\dot{\varepsilon}_1^{\text{vp}} + \frac{\langle \bar{\phi}_1 \rangle}{\eta_1} \text{sign}(N_1 - \chi_1 A) = 0 \Rightarrow \dot{\varepsilon}_1^{\text{vp}} = \dot{\gamma}_1 \text{sign}(N_1 - \chi_1 A) \\ \frac{\partial \bar{\mathcal{L}}_1}{\partial \bar{q}_1} &= -A \dot{\zeta}_1 + A \frac{\langle \bar{\phi}_1 \rangle}{\eta_1} = 0 \Rightarrow \dot{\zeta}_1 = \dot{\gamma}_1 \\ \frac{\partial \bar{\mathcal{L}}_2}{\partial N_2} &= -\dot{\gamma}_{12}^{\text{vp}} + \frac{\langle \bar{\phi}_2 \rangle}{\eta_2} \text{sign}(N_2 - \chi_2 A) = 0 \Rightarrow \dot{\gamma}_{12}^{\text{vp}} = \dot{\gamma}_2 \text{sign}(N_2 - \chi_2 A) \\ \frac{\partial \bar{\mathcal{L}}_2}{\partial \bar{q}_2} &= -A \dot{\zeta}_2 + A \frac{\langle \bar{\phi}_2 \rangle}{\eta_2} = 0 \Rightarrow \dot{\zeta}_2 = \dot{\gamma}_2 \\ \frac{\partial \bar{\mathcal{L}}_3}{\partial N_3} &= -\dot{\gamma}_{13}^{\text{vp}} + \frac{\langle \bar{\phi}_3 \rangle}{\eta_3} \text{sign}(N_3 - \chi_3 A) = 0 \Rightarrow \dot{\gamma}_{13}^{\text{vp}} = \dot{\gamma}_3 \text{sign}(N_3 - \chi_3 A) \\ \frac{\partial \bar{\mathcal{L}}_3}{\partial \bar{q}_3} &= -A \dot{\zeta}_3 + A \frac{\langle \bar{\phi}_3 \rangle}{\eta_3} = 0 \Rightarrow \dot{\zeta}_3 = \dot{\gamma}_3\end{aligned}$$

where we denoted the viscoplastic multiplier $\dot{\gamma}_i = \langle \bar{\phi}_i \rangle / \eta_i$.

3.4 Local computation

At iterative sweep $(j + 1)$, the values of the previous iteration for nodal displacements, rotations, and voltage are known: $\mathbf{a}_{a,n+1}^{u_i(j)}$, $\mathbf{a}_{a,n+1}^{\varphi_i(j)}$, $\mathbf{a}_{a,n+1}^{V_i(j)}$. First, the electric field is calculated in order to obtain the value of the polarization multiplier. The previous stored value of axial force $N_{1,n}$ is used as well if the switching model 2 is activated.

A trial step, denoted by superscript tr, is assumed as elastic, where all viscoplastic variables remain unchanged from the converged values in the previous time step:

$$\begin{aligned}\varepsilon_{1,n+1}^{\text{vp,tr}} &= \varepsilon_{1,n}^{\text{vp}}; & \gamma_{12,n+1}^{\text{vp,tr}} &= \gamma_{12,n}^{\text{vp}}; & \gamma_{13,n+1}^{\text{vp,tr}} &= \gamma_{13,n}^{\text{vp}}; & \bar{\zeta}_{i,n+1}^{\text{tr}} &= \bar{\zeta}_{i,n} \\ \bar{q}_{i,n+1}^{\text{tr}} &= \bar{q}_{i,n}; & \alpha_{i,n+1}^{\text{tr}} &= \alpha_{i,n}; & \bar{\zeta}_{i,n+1}^{\text{tr}} &= \bar{\zeta}_{i,n}; & \bar{q}_{i,n+1}^{\text{tr}} &= \bar{q}_{i,n}\end{aligned}$$

The computation is followed by the calculation of the axial strain, modified by polarization material properties in (15), and the constitutive terms in (16). The trial forces, moments, and the electric charge are computed with so chosen previous values as follows:

$$\begin{aligned}N_1^{\text{tr}} &= \check{E}A \left(\sum_{a=1}^2 \mathcal{B}_a \mathbf{a}_{a,n+1}^{u_1} - \varepsilon_{1,n}^{\text{vp}} - \varepsilon_{1,n+1}^{\text{r}} + \bar{\mathcal{G}}\alpha_{1,n} \right) + e_{11}A \sum_{a=1}^2 \mathcal{B}_a a_{a,n+1}^V \\ N_2^{\text{tr}} &= k_c GA \left(\sum_{a=1}^2 \mathcal{B}_a \mathbf{a}_{a,n+1}^{u_2} - \mathcal{N}_a \mathbf{a}_a^{\varphi_3} - \gamma_{12,n}^{\text{vp}} + \bar{\mathcal{G}}\alpha_{2,n} \right); \\ N_3^{\text{tr}} &= k_c GA \left(\sum_{a=1}^2 \mathcal{B}_a \mathbf{a}_{a,n+1}^{u_3} + \mathcal{N}_a \mathbf{a}_a^{\varphi_2} - \gamma_{13,n}^{\text{vp}} + \bar{\mathcal{G}}\alpha_{3,n} \right); \\ M_1^{\text{tr}} &= GJ \sum_{a=1}^2 \mathcal{B}_a \mathbf{a}_{a,n+1}^{\varphi_1} \\ M_2^{\text{tr}} &= \check{E}I \sum_{a=1}^2 \mathcal{B}_a \mathbf{a}_{a,n+1}^{\varphi_2} \\ M_3^{\text{tr}} &= \check{E}I \sum_{a=1}^2 \mathcal{B}_a \mathbf{a}_{a,n+1}^{\varphi_3} \\ Q_1^{\text{tr}} &= e_{11}A \left(\sum_{a=1}^2 \mathcal{B}_a \mathbf{a}_{a,n+1}^{u_1} - \varepsilon_{1,n}^{\text{vp}} - \varepsilon_{1,n+1}^{\text{r}} + \bar{\mathcal{G}}\alpha_{1,n} \right) - \varepsilon_1 A \sum_{a=1}^2 \mathcal{B}_a \mathbf{a}_{a,n+1}^V\end{aligned}$$

Plasticity is triggered when the yield limit $N_{i,y}$ is reached. The yield criteria is tested with trial values:

$$\bar{\phi}_{i,n+1}^{\text{tr}} = |N_{i,n+1}^{\text{tr}} - \chi_{i,n+1}^{\text{tr}} A| - (N_{i,y} - \bar{q}_{i,n+1}^{\text{tr}} A)$$

If $\bar{\phi}_{i,n+1}^{\text{tr}} \leq 0$, the hypothesis of elastic regime is correct and all local variables remain the same as in the previous time step. Otherwise, the viscoplastic step is accepted.

3.5 Viscoplastic regime

In the case that $\bar{\phi}_{i,n+1}^{\text{tr}} > 0$, the evolution of the viscoplastic variables defined in (30) is

computed by an implicit time integration scheme. The following development is an extension to the one presented in Ibrahimbegovic *et al.* (1998) Ibrahimbegovic (1997). This computation is analogous for any local directions, taking into account the equivalent role of the internal variables for all directions. For direction 1 we have:

$$\begin{aligned}\varepsilon_{1,n+1}^{\text{vp}} &= \varepsilon_{1,n}^{\text{vp}} + \bar{\gamma}_{1,n+1} \text{sign}(N_{1,n+1} - \chi_{1,n+1}A) \\ \bar{\zeta}_{1,n+1} &= \bar{\zeta}_{1,n} + \bar{\gamma}_{1,n+1}; \\ \bar{q}_{1,n+1} &= -H_{is}\bar{\zeta}_{1,n+1} \\ \chi_{1,n+1} &= \chi_{1,n} + H_{l,1}\bar{\gamma}_{1,n+1} \text{sign}(N_{1,n+1} - \chi_{1,n+1}A) - H_{n,1}\bar{\gamma}_{1,n+1}\chi_{1,n+1}; \\ N_{1,n+1} &= N_{1,n}^{\text{tr}} - \check{E}A\bar{\gamma}_{1,n+1} \text{sign}(N_{1,n+1} - \chi_{1,n+1}A)\end{aligned}$$

Subtracting $\chi_{1,n+1}$ multiplied by the area to $N_{1,n+1}$, introducing the null term

$$\bar{\gamma}_{1,n+1}H_{n,1}(-N_{1,n+1} + N_{1,n}^{\text{tr}} - \check{E}A\bar{\gamma}_{1,n+1} \text{sign}(N_{1,n+1} - \chi_{1,n+1}A))$$

and further simplifying:

$$\begin{aligned}(N_{1,n+1} - \chi_{1,n+1}A) &= [(1 + \bar{\gamma}_{1,n+1}H_{n,1})N_{1,n}^{\text{tr}} - \chi_{1,n}A] - \\ &\bar{\gamma}_{1,n+1}[(\check{E}A + H_{l,1}A) \text{sign}(N_{1,n+1} - \chi_{1,n+1}A) + \\ &H_{n,1}(N_{1,n+1} - \chi_{1,n+1}A) + H_{n,1}\check{E}A\bar{\gamma}_{1,n+1} \text{sign}(N_{1,n+1} - \chi_{1,n+1}A)]\end{aligned}$$

By using the identity $a = |a|\text{sign}(a)$, we can recast to the previous equation in equivalent format:

$$\begin{aligned}\{|N_{1,n+1} - \chi_{1,n+1}A| + \bar{\gamma}_{1,n+1}[(\check{E}A + H_{l,1}A) + \\ H_{n,1}|N_{1,n+1} - \chi_{1,n+1}A| + H_{n,1}\check{E}A\bar{\gamma}_{1,n+1}]\} \text{sign}(N_{1,n+1} - \chi_{1,n+1}A) = \\ |(1 + \bar{\gamma}_{1,n+1}H_{n,1})N_{1,n}^{\text{tr}} - \chi_{1,n}A| \text{sign} [(1 + \bar{\gamma}_{1,n+1}H_{n,1})N_{1,n}^{\text{tr}} - \chi_{1,n}A]\end{aligned}$$

By taking into account that all terms inside the braces and absolute values are positive, the following relation with respect to the sign operator can be established:

$$\text{sign}(N_{1,n+1} - \chi_{1,n+1}A) = \text{sign} [(1 + \bar{\gamma}_{1,n+1}H_{n,1})N_{1,n}^{\text{tr}} - \chi_{1,n}A]$$

Furthermore, we conclude that the terms multiplying both signs in (37) must also be equal. Introducing the definition of viscoplastic multiplier, we can identify the yield criteria:

$$\bar{\phi}_{i,n+1} = |N_{1,n+1} - \chi_{1,n+1}A| - (N_{i,y} - \bar{q}_{1,n+1}) = \bar{\gamma}_{1,n+1} \frac{\eta_i}{\Delta t}$$

where Δt is the current time step. Thus, the norm $|N_{1,n+1} - \chi_{1,n+1}A|$ in (37) can be replaced now, resulting in:

$$\begin{aligned} |(1 + \bar{\gamma}_{1,n+1}H_{n,1})N_{1,n}^{\text{tr}} - \chi_{1,n}A| - (N_{1,y} + H_{is}A\bar{\zeta}_{1,n}) - \bar{\gamma}_{1,n+1}[\check{E}A + H_{l,1}A \\ + H_{is}A + \frac{\eta_1}{\Delta t} + H_{n,1}(N_{1,y} + H_{is}A\bar{\zeta}_{1,n}) + \bar{\gamma}_{1,n+1}H_{n,1}(\frac{\eta_1}{\Delta t} + \check{E}A + H_{is}A)] = 0\end{aligned}$$

The Newton-Raphson iterative method is used to solve for $\bar{\gamma}_{1,n+1}$ the previous from this quadratic equation. Such an iterative method requires a good guess for the initial value so that the positive final value is found. A very good initial guess can be found in Hadzalic *et al.* (2019), where the following expression is obtained for explicit back-stress Armstrong-Frederick:

$$\bar{\gamma}_{1,n+1}^{(0)} = \frac{\bar{\phi}_{i,n+1}^{\text{tr}}}{\check{E}A + H_{is}A + H_{l,1}A + \frac{\eta_i}{\Delta t} - H_{n,1}A\chi_{1,n}}$$

3.6 Global step computation

The starting point for the global solution step implementation is provided by the weak form of the equilibrium equations (11), where the approximations (??) and (??) have been introduced:

$$\begin{aligned} \int_0^L \mathcal{B}_a w_a^{u_i} N_{i,n+1} dx_1 - w_a^{u_i} \bar{N}_i|_{\Gamma_N} &= 0 \\ \int_0^L \mathcal{B}_a w_a^{\varphi_i} M_{i,n+1} dx_1 - w_a^{\varphi_i} \bar{M}_i|_{\Gamma_M} &= 0 \\ \int_0^L \mathcal{B}_a w_a^V Q_{1,n+1} dx_1 - w_a^V \bar{Q}_1|_{\Gamma_Q} &= 0 \end{aligned}$$

with $w_a^{u_i}$, $w_a^{\varphi_i}$, and w_a^V as the nodal values of the corresponding virtual fields. The kinematic admissibility requires that these nodal values are set to zero if a Dirichlet boundary condition is applied to node a . The corresponding residual is obtained by removing the virtual degrees of freedom in (42) above resulting with:

$$\begin{aligned} \mathcal{R}_{a,n+1}^{u_i} &= \int_0^L \mathcal{B}_a N_{i,n+1} dx_1 - \bar{N}_i|_{\Gamma_N} = 0 \\ \mathcal{R}_{a,n+1}^{\varphi_i} &= \int_0^L \mathcal{B}_a M_{i,n+1} dx_1 - \bar{M}_i|_{\Gamma_M} = 0 \\ \mathcal{R}_{a,n+1}^V &= \int_0^L \mathcal{B}_a Q_{1,n+1} dx_1 - \bar{Q}_1|_{\Gamma_Q} = 0 \end{aligned}$$

where the forces, moments and electric charge are defined as:

$$\begin{aligned} N_1 &= \check{E}A \left(\sum_{a=1}^2 \mathcal{B}_a \mathbf{a}_{a,n+1}^{u_1} - \varepsilon_{1,n+1}^{vp} - \varepsilon_{1,n+1}^r + \bar{\mathcal{G}}\alpha_{1,n+1} \right) + e_{11}A \sum_{a=1}^2 \mathcal{B}_a \mathbf{a}_{a,n+1}^V \\ N_2 &= k_c GA \left(\sum_{a=1}^2 \mathcal{B}_a \mathbf{a}_{a,n+1}^{u_2} - \mathcal{N}_a \mathbf{a}_{a,n+1}^{\varphi_3} - \gamma_{12,n+1}^{vp} + \bar{\mathcal{G}}\alpha_{2,n+1} \right) \\ N_3 &= k_c GA \left(\sum_{a=1}^2 \mathcal{B}_a \mathbf{a}_{a,n+1}^{u_3} + \mathcal{N}_a \mathbf{a}_{a,n+1}^{\varphi_2} - \gamma_{13,n+1}^{vp} + \bar{\mathcal{G}}\alpha_{3,n+1} \right) \\ M_1 &= GJ \sum_{a=1}^2 \mathcal{B}_a \mathbf{a}_{a,n+1}^{\varphi_1} \\ M_2 &= \check{E}I \sum_{a=1}^2 \mathcal{B}_a \mathbf{a}_{a,n+1}^{\varphi_2} \\ M_3 &= \check{E}I \sum_{a=1}^2 \mathcal{B}_a \mathbf{a}_{a,n+1}^{\varphi_3} \\ Q_1 &= e_{11}A \left(\sum_{a=1}^2 \mathcal{B}_a \mathbf{a}_{a,n+1}^{u_1} - \varepsilon_{1,n+1}^{vp} - \varepsilon_{1,n+1}^r + \bar{\mathcal{G}}\alpha_{1,n+1} \right) - \epsilon_1 A \sum_{a=1}^2 \mathcal{B}_a \mathbf{a}_{a,n+1}^V \end{aligned}$$

In order to solve this set of global nonlinear equations, we use the Newton-Raphson iterative method:

$$\mathbf{R}_{a,n+1}^{(i+1)} = 0 \Rightarrow \mathbf{R}_{a,n+1}^{(i)} + \left. \frac{\partial \mathbf{R}_{a,n+1}}{\partial \mathbf{a}_{b,n+1}} \right|^{(i)} \Delta \mathbf{a}_{b,n+1}^{(i)} = 0$$

At each iterative sweep, we can perform the corresponding state variable updates according to:

$$\mathbf{a}_{b,n+1}^{(i+1)} = \mathbf{a}_{b,n+1}^{(i)} + \Delta \mathbf{a}_{b,n+1}^{(i)}$$

We note that within each time step, the starting guess in the first iteration is assumed to be the converged value at the previous step:

$$\mathbf{a}_{b,n+1}^{(0)} = \mathbf{a}_{b,n}$$

The derivative term in (45) is the stiffness matrix, which is constructed in the appropriate manner depending on the local regime that the particular bar is undergoing.

4. Numerical examples

In this section, we present the results of several illustrative numerical simulations. All computations were performed by a research version of computer code FEAP 8.4 (see Taylor 2012)

4.1 Single-crystal simulation

In this example, a single beam of length $L = 0.1$ m is simulated to obtain the characteristic hysteresis loops. This beam is clamped on the left side and subjected to ground voltage. On the right side, a variable voltage is set in terms of a triangular force, with maximum and minimum values of 300 and -300 V. The material properties are gathered in Table 1.

The results are displayed in Fig. 9. On the left, the electric charge Q_1 has the characteristic loop for single crystal. The slope does not change since the non-polarized and the polarized value of the electric permittivity are the same. Also, the value of Q_1 at $E = 0$ is the value of $P_s A$. Fig. 9 Electric charge and strain obtained for the beam of the numerical example.

On the right, the computed strain history is plotted showing a typical butterfly loop. Notice that the strain takes negative values when the electric field is close to the coercive value; in other words, when the beam is close to the change of polarization.

Table 1 Material properties for the material used in the single crystal polarization simulation

Property	Units	Value
First stiffness term \tilde{E}	GPa	100
Poisson's coefficient ν	–	0.3
Permittivity ϵ_1	C/V m	1.5×10^{-9}
Spontaneous polarization P_s	C/m ²	2×10^{-5}
Piezoelectric term e_{11}	C/m ²	5×10^{-7}
Non-polarized spontaneous strain ϵ_1^{NP}	–	-1×10^{-5}
Polarized spontaneous strain ϵ_1^{P}	–	4×10^{-5}
Cross-section Area A	m ²	0.5

Table 2 Material properties for the material used in the macro-model.

Property	Units	Value
First stiffness term \check{E}	GPa	68
Poisson's coefficient ν	–	0.3
Permittivity ϵ_1	C/V m	56.3×10^{-9}
Spontaneous polarization P_s	C/m ²	0.25
Piezoelectric term e_{11}	C/m ²	1.18×10^{-9}
Coercive Electric Field E_c	V/m	0.36×10^6

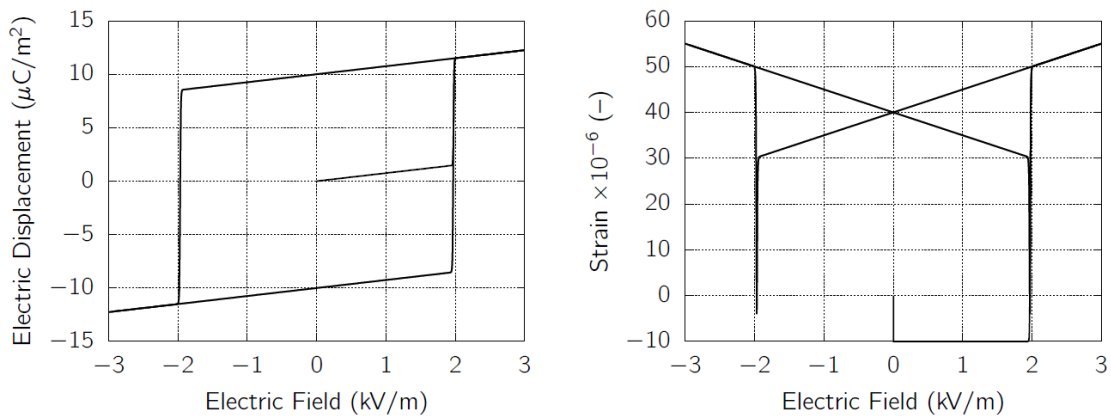


Fig. 9 Mesh used for the numerical examples. Left, Voronoi cell representation; right, lattice model, dual to Voronoi

We note that even though the proposed lattice model may seem quite simple, it is capable of capturing the behavior of a heterogeneous material. We can see further in the next example.

4.2 Macro-model subjected to cyclic electric field applied in vertical direction

The geometry of the numerical example in this section is a cube, with sides of 20 cm as can be seen in Fig. 10. On the left, the Voronoi representation (Nikolić *et al.* 2018, Nikolic and Ibrahimbegovic 2015, Ibrahimbegovic *et al.* 2020) of the cube is pictured, where the different colors show the boundary faces of the Voronoi cells. On the right, the corresponding mesh of lattice beams is depicted. The material properties are extracted from Hwang *et al.* (1995), and given in Table 2.

The top and bottom faces have prescriptions of the voltage of $V = 0$ and $V = V_t(t)$, respectively. The voltage at the top is triangular, starting with a value of 0 increasing to $V_{\max} = 0.2\text{MV}$, then decreasing $-V_{\max}$ and finally returning to V_{\max} . In planes $x_1 = 0$, $x_2 = 0$, and $x_3 = 0$, the corresponding perpendicular displacement is prescribed to simulate symmetry boundary conditions for one eighth of the specimen. The Neumann boundary condition is also set introducing a constant compressive force. Rotation degrees of freedom are left free. All switches are set initially to zero.

The electric and mechanic variables calculated with the beam model have to be expressed in the global frame and averaged with the volume in order to obtain the corresponding macro response of

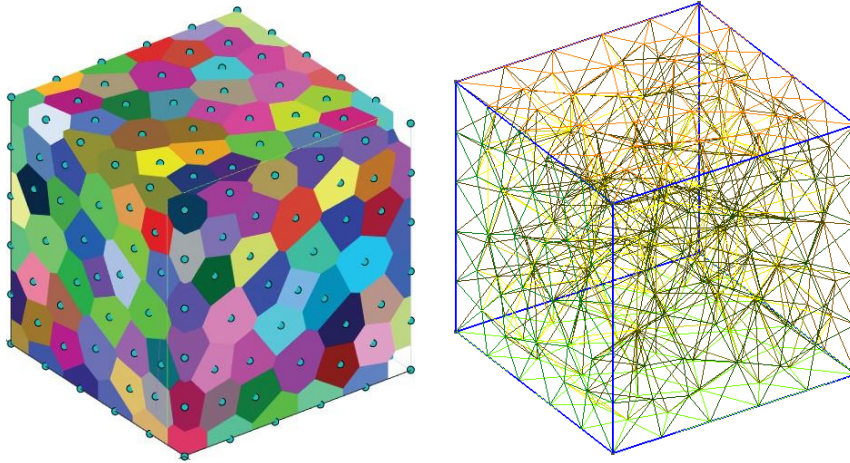


Fig. 10 Mesh used for the numerical examples, Left, Voronoi cell representation, right, lattice model, dual to Voronoi

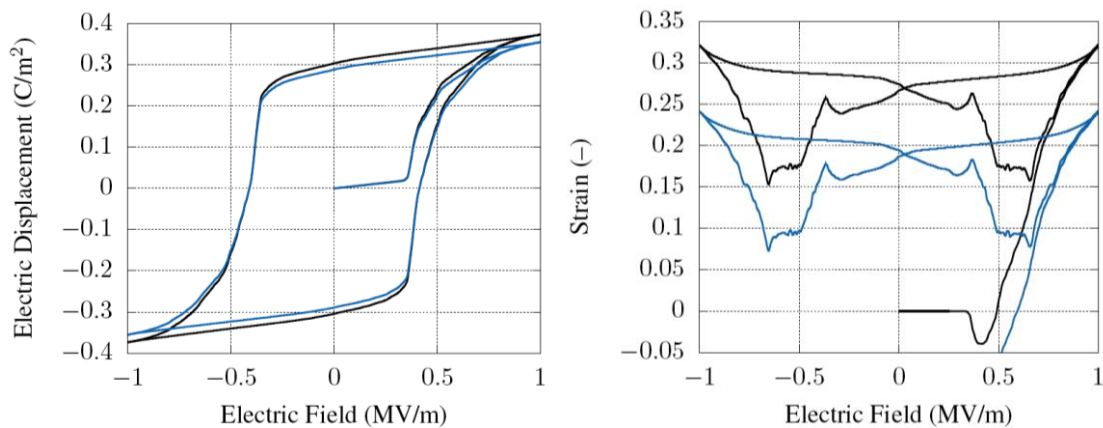


Fig. 11 Averaged vertical electric displacement and strain obtained for the numerical example

the material by using:

$$\bar{\xi} = \frac{\int_{\Omega^e} \xi d\Omega}{\int_{\Omega^e} d\Omega}$$

Fig. 11 Averaged vertical electric displacement and strain obtained for the numerical example

In Fig. 11, such an averaged response computed in this numerical example is plotted, where the typical hysteresis loops for electric displacement and strain are given on left and right, respectively. The curves in black are obtained without the compressive force, whereas the blue ones have the imposed boundary condition representing the compressive force. The difference lies in the number of beams that get polarized. The compressive force makes it more difficult to get polarized as depicted in (19).

The averaged strain is affected as well by the introduction of the compressive force. The strain is almost an offset of the one without the force. The shape of the butterfly loop is not as perfect as in the single-crystal simulation. Namely, the minimum stress is not close to zero, and the

spontaneous polarization is a little bit higher than the expected value, according to Hwang *et al.* (1995). We can see here one of the limitations of this method is that cannot capture transversal effects with accuracy, but the axial variables are close to the ones of the continuum model.

5. Conclusions

This paper presents a theoretical micro-model formulation that couples ferroelectricity, viscoplasticity. Each of the elements simulates a single crystal of the whole macrostructure that can be polarized in the axial or transversal direction. This feature makes the element suitable for multi-scale computations since it can replicate the behavior of the macro response of ferroelectric materials by introducing the properties of a single crystal.

The introduction of an embedded discontinuity model in future versions of the element could be crucial in applications under significant or cyclic loadings of any kind, not only mechanical. Potential current and future applications of this type include microsensors that measure outside their usual range, overcharged actuators, solid-state batteries under charging that undergo large temperature gradients.

The numerical examples presented in this work show a good agreement between experiments and the response of the model. In some cases, the polarization switching model 1 could be enough to capture the axial response accurately, although model 2 is not much more expensive in terms of computation resources.

Acknowledgments

This article was supported jointly by Hauts-de-France Region (CR Picardie) (120-2015RDISTRUCT-000010 and RDISTRUCT-000010) and EU funding (FEDER) for Chair of Mechanics (120-2015-RDISTRUCTF-000010 and RDISTRUCTI-000004), IUF-Institut Universitaire de France and by Germaine de Staël Collaborative Program between France and Switzerland. All this support is gratefully acknowledged.

References

- Abdollahi, A. and Arias, I. (2015), "Phase-field modeling of fracture in ferroelectric materials", *Arch. Comput. Meth. Eng.*, **22**(2), 153-181. <https://doi.org/10.1007/s11831-014-9118-8>.
- Armero, F. and Garikipati, K. (1996), "An analysis of strong discontinuities in multiplicative finite strain plasticity and their relation with the numerical simulation of strain localization in solids", *Int. J. Solid. Struct.*, **33**(20-22), 2863-2885. [https://doi.org/10.1016/0020-7683\(95\)00257-X](https://doi.org/10.1016/0020-7683(95)00257-X).
- Balanis, C.A. (1999), *Advanced Engineering Electromagnetics*, John Wiley & Sons.
- Belytschko, T., Fish, J. and Engelmann, B. E. (1988), "A finite element with embedded localization zones", *Comput. Meth. Appl. Mech. Eng.*, **70**(1), 59-89. [https://doi.org/10.1016/0045-7825\(88\)90180-6](https://doi.org/10.1016/0045-7825(88)90180-6).
- Brancherie, D. and Ibrahimbegovic, A. (2009), "Novel anisotropic continuum-discrete damage model capable of representing localized failure of massive structures: Part I: Theoretical formulation and numerical implementation", *Eng. Comput.*, **26**(1/2), 100-127. <https://doi.org/10.1108/02644400910924825>.
- Bui, N.N., Ngo, M., Nikolic, M., Brancherie, D. and Ibrahimbegovic, A. (2014), "Enriched Timoshenko beam finite element for modeling bending and shear failure of reinforced concrete frames", *Comput. Struct.*, **143**,

- 9-18. <https://doi.org/10.1016/j.compstruc.2014.06.004>.
- Chen, W. and Lynch, C.S. (1998), "A micro-electro-mechanical model for polarization switching of ferroelectric materials", *Acta Materialia*, **46**(15), 5303-5311. [https://doi.org/10.1016/S1359-6454\(98\)00207-9](https://doi.org/10.1016/S1359-6454(98)00207-9).
- Damjanovic, D. (2006), *Hysteresis in Piezoelectric and Ferroelectric Materials*, No. BOOK_CHAP, Academic Press.
- Daniel, L., Hubert, O. and Billardon, R. (2004), "Homogenisation of magneto-elastic behaviour: from the grain to the macro scale", *Comput. Appl. Math.*, **23**, 285-308.
- Daniel, L., Hubert, O., Buiron, N. and Billardon, R. (2008), "Reversible magneto-elastic behavior: A multiscale approach", *J. Mech. Phys. Solid.*, **56**(3), 1018-1042. <https://doi.org/10.1016/j.jmps.2007.06.003>.
- Daniel, L., Rezik, M. and Hubert, O. (2014), "A multiscale model for magneto-elastic behaviour including hysteresis effects", *Arch. Appl. Mech.*, **84**(9), 1307-1323. <https://doi.org/10.1007/s00419-014-0863-9>.
- De Jong, M., Chen, W., Geerlings, H., Asta, M. and Persson, K.A. (2015), "A database to enable discovery and design of piezoelectric materials", *Scientif. Data*, **2**(1), 1-13. <https://doi.org/10.1038/sdata.2015.53>.
- Do, X.N., Ibrahimbegovic, A. and Brancherie, D. (2017), "Dynamics framework for 2D anisotropic continuum-discrete damage model for progressive localized failure of massive structures", *Comput. Struct.*, **183**, 14-26. <https://doi.org/10.1016/j.compstruc.2017.01.011>.
- Hadzalic, E., Ibrahimbegovic, A. and Dolarevic, S. (2019), "Theoretical formulation and seamless discrete approximation for localized failure of saturated poro-plastic structure interacting with reservoir", *Comput. Struct.*, **214**, 73-93. <https://doi.org/10.1016/j.compstruc.2019.01.003>.
- Huber, J.E., Fleck, N.A. and McMeeking, R.M. (1999), "A crystal plasticity model for ferroelectrics", *Ferroelec.*, **228**(1), 39-52. <https://doi.org/10.1080/00150199908226124>.
- Hwang, S.C., Lynch, C.S. and McMeeking, R.M. (1995), "Ferroelectric/ferroelastic interactions and a polarization switching model", *Acta Metallurgica et Materialia*, **43**(5), 2073-2084. [https://doi.org/10.1016/0956-7151\(94\)00379-V](https://doi.org/10.1016/0956-7151(94)00379-V).
- Ibrahimbegovic, A. (1997), "Théorie géométriquement exacte des coques en rotations finies et son implantation éléments finis", *Revue Européenne des Éléments Finis*, **6**(3), 263-335. <https://doi.org/10.1080/12506559.1997.10511273>.
- Ibrahimbegovic, A. (2009), *Nonlinear Solid Mechanics: Theoretical Formulations and Finite Element Solution Methods*, Vol. 160, Springer Science & Business Media.
- Ibrahimbegovic, A. and Brancherie, D. (2003), "Combined hardening and softening constitutive model of plasticity: precursor to shear slip line failure", *Comput. Mech.*, **31**(1), 88-100. <https://doi.org/10.1007/s00466-002-0396-x>.
- Ibrahimbegovic, A. and Delaplace, A. (2003), "Microscale and mesoscale discrete models for dynamic fracture of structures built of brittle material", *Comput. Struct.*, **81**(12), 1255-1265. [https://doi.org/10.1016/S0045-7949\(03\)00040-3](https://doi.org/10.1016/S0045-7949(03)00040-3).
- Ibrahimbegovic, A. and Melnyk, S. (2007), "Embedded discontinuity finite element method for modeling of localized failure in heterogeneous materials with structured mesh: an alternative to extended finite element method", *Comput. Mech.*, **40**(1), 149-155. <https://doi.org/10.1007/s00466-006-0091-4>.
- Ibrahimbegovic, A. and Wilson, E.L. (1991), "A modified method of incompatible modes", *Commun. Appl. Numer. Meth.*, **7**(3), 187-194. <https://doi.org/10.1002/cnm.1630070303>.
- Ibrahimbegović, A., Gharzeddine, F. and Chorfi, L. (1998), "Classical plasticity and viscoplasticity models reformulated: theoretical basis and numerical implementation", *Int. J. Numer. Meth. Eng.*, **42**(8), 1499-1535. [https://doi.org/10.1002/\(SICI\)1097-0207\(19980830\)42:8<1499::AID-NME443>3.0.CO;2-X](https://doi.org/10.1002/(SICI)1097-0207(19980830)42:8<1499::AID-NME443>3.0.CO;2-X).
- Ibrahimbegovic, A., Matthies, H.G. and Karavelić, E. (2020), "Reduced model of macro-scale stochastic plasticity identification by Bayesian inference: Application to quasi-brittle failure of concrete", *Comput. Meth. Appl. Mech. Eng.*, **372**, 113428. <https://doi.org/10.1016/j.cma.2020.113428>.
- Karavelić, E., Ibrahimbegovic, A. and Dolarević, S. (2019), "Multi-surface plasticity model for concrete with 3D hardening/softening failure modes for tension, compression and shear", *Comput. Struct.*, **221**, 74-90. <https://doi.org/10.1016/j.compstruc.2019.05.009>.
- Keip, M.A. and Schröder, J. (2011), "A ferroelectric and ferroelastic microscopic switching criterion for

- tetragonal ferroelectrics”, *PAMM*, **11**(1), 475-476. <https://doi.org/10.1002/pamm.201110229>.
- Labusch, M., Keip, M.A., Shvartsman, V.V., Lupascu, D.C. and Schröder, J. (2016), “On the influence of ferroelectric polarization states on the Magneto-electric coupling in two-phase composites”, *Technische Mechanik-Eur. J. Eng. Mech.*, **36**(1-2), 73-87. <https://doi.org/10.24352/UB.OVGU-2017-011>.
- McMeeking, R.M. and Hwang, S.C. (1997), “On the potential energy of a piezoelectric inclusion and the criterion for ferroelectric switching”, *Ferroelec.*, **200**(1), 151-173. <https://doi.org/10.1080/00150199708008603>.
- McMeeking, R.M. and Landis, C.M. (2002), “A phenomenological multi-axial constitutive law for switching in polycrystalline ferroelectric ceramics”, *Int. J. Eng. Sci.*, **40**(14), 1553-1577. [https://doi.org/10.1016/S0020-7225\(02\)00033-2](https://doi.org/10.1016/S0020-7225(02)00033-2).
- Medić, S., Dolarević, S. and Ibrahimbegovic, A. (2013), “Beam model refinement and reduction”, *Eng. Struct.*, **50**, 158-169. <https://doi.org/10.1016/j.engstruct.2012.10.004>.
- Miehe, C., Rosato, D. and Kiefer, B. (2011), “Variational principles in dissipative electro-magneto-mechanics: A framework for the macro-modeling of functional materials”, *Int. J. Numer. Meth. Eng.*, **86**(10), 1225-1276. <https://doi.org/10.1002/nme.3127>.
- Moreno-Navarro, P., Ibrahimbegovich, A. and Perez-Aparicio, J.L. (2018), “Linear elastic mechanical system interacting with coupled thermo-electro-magnetic fields”, *Couple. Syst. Mech.*, **7**(1), 5-25. <https://doi.org/10.12989/csm.2018.7.1.005>
- Ngo, V.M., Ibrahimbegović, A. and Brancherie, D. (2013), “Model for localized failure with thermo-plastic coupling: theoretical formulation and ED-FEM implementation”, *Comput. Struct.*, **127**, 2-18. <https://doi.org/10.1016/j.compstruc.2012.12.013>.
- Nikolic, M. and Ibrahimbegovic, A. (2015), “Rock mechanics model capable of representing initial heterogeneities and full set of 3D failure mechanisms”, *Comput. Meth. Appl. Mech. Eng.*, **290**, 209-227. <https://doi.org/10.1016/j.cma.2015.02.024>.
- Nikolic, M., Ibrahimbegovic, A. and Miscevic, P. (2016), “Discrete element model for the analysis of fluid-saturated fractured poro-plastic medium based on sharp crack representation with embedded strong discontinuities”, *Comput. Meth. Appl. Mech. Eng.*, **298**, 407-427. <https://doi.org/10.1016/j.cma.2015.10.009>.
- Nikolić, M., Karavelić, E., Ibrahimbegovic, A. and Mišćević, P. (2018), “Lattice element models and their peculiarities”, *Arch. Comput. Meth. Eng.*, **25**(3), 753-784. <https://doi.org/10.1007/s11831-017-9210-y>.
- Ostoja-Starzewski, M. (2002), “Lattice models in micromechanics”, *Appl. Mech. Rev.*, **55**(1), 35-60. <https://doi.org/10.1115/1.1432990>.
- Palma, R., Pérez-Aparicio, J.L. and Taylor, R.L. (2018), “Dissipative finite-element formulation applied to piezoelectric materials with the Debye memory”, *IEEE/ASME Tran. Mechatron.*, **23**(2), 856-863. <https://doi.org/10.1109/TMECH.2018.2792308>.
- Rowe, D.M. (2018), *Thermoelectrics Handbook: Macro to Nano*, CRC Press.
- Rukavina, I., Ibrahimbegovic, A., Do, X.N. and Markovic, D. (2019), “ED-FEM multi-scale computation procedure for localized failure”, *Couple. Syst. Mech.*, **8**(2), 111-127. <https://doi.org/10.12989/csm.2019.8.2.111>.
- Said, S.M., Sabri, M.F.M. and Salleh, F. (2017), *Ferroelectrics and their Applications, Reference Module in Materials Science and Materials Engineering*, Elsevier.
- Saksala, T., Brancherie, D., Harari, I. and Ibrahimbegovic, A. (2015), “Combined continuum damage-embedded discontinuity model for explicit dynamic fracture analyses of quasi-brittle materials”, *Int. J. Numer. Meth. Eng.*, **101**(3), 230-250. <https://doi.org/10.1002/nme.4814>.
- Schlangen, E. and Garboczi, E.J. (1997), “Fracture simulations of concrete using lattice models: computational aspects”, *Eng. Fract. Mech.*, **57**(2-3), 319-332. [https://doi.org/10.1016/S0013-7944\(97\)00010-6](https://doi.org/10.1016/S0013-7944(97)00010-6).
- Schröder, J. and Romanowski, H. (2005), “A thermodynamically consistent mesoscopic model for transversely isotropic ferroelectric ceramics in a coordinate-invariant setting”, *Arch. Appl. Mech.*, **74**(11), 863-877. <https://doi.org/10.1007/s00419-005-0412-7>.
- Simo, J.C., Oliver, J.A.V.I.E.R. and Armero, F. (1993), “An analysis of strong discontinuities induced by

- strain-softening in rate-independent inelastic solids”, *Comput. Mech.*, **12**(5), 277-296.
<https://doi.org/10.1007/BF00372173>.
- Taylor, R.L. (2012), FEAP-A Finite Element Analysis Program, Version 8.4 Theory Manual.
- White Jr. B.E. (2008), “Energy-harvesting devices: Beyond the battery”, *Nat. Nanotechnol.*, **3**(2), 71.
- Zienkiewicz, O.C. and Taylor, R.L. (2005), *The Finite Element Method, Vols. I, II, III*, Elsevier.